

Evolution of Pearlite Microstructure in Low-Carbon Cast Microalloyed Steel Due to the Addition of La and Ce



H. TORKAMANI, SH. RAYGAN, C. GARCIA-MATEO, J. RASSIZADEHGHANI, Y. PALIZDAR, and D. SAN-MARTIN

The effects of rare earth elements (RE) addition on the pearlite microstructure in low-carbon microalloyed steels have been investigated under two heat treatment conditions: (1) a normalizing treatment (as a conventional heat treatment used industrially to obtain the final mechanical properties of such steels), and (2) an isothermal treatment at 650 °C. This research reports the following effects due to the addition of RE: (i) refinement of the nodule and colony size of pearlite along with the ferrite grain size in the normalized condition, without a significant change in the volume fraction of pearlite. This microstructural refinement observed at room temperature is a consequence of the refinement of cast and austenitic microstructures formed during cooling in the presence of RE; (ii) the interlamellar spacing of pearlite isothermally transformed at 650 °C, as observed by SEM and TEM, is effectively reduced in the RE-added steel. This is likely due to two different effects combined: (i) direct influence of RE on atom carbon diffusion; and (ii) pearlite growth being boundary diffusion controlled by RE partitioning.

<https://doi.org/10.1007/s11661-018-4796-8>

© The Minerals, Metals & Materials Society and ASM International 2018

I. INTRODUCTION

MOST of the common air-cooled cast structural steels have a mixed ferrite-pearlite microstructure.^[1] The formation of pearlite is a process during which alternate layers of ferrite and cementite develop. The neighboring ferrite and cementite lamellae grow parallel to each other sharing a transformation front with austenite. As the ferrite grows, the excess carbon partitions into the austenite which will be absorbed by the adjacent cementite and *vice versa*. This cooperative growth creates a colony. As the colony grows, new lamella may nucleate from its sides and take a different growth direction. In this way, new colonies with different lamellae orientation from the adjacent colonies are generated, and eventually a larger reacted volume

known as a pearlite nodule is formed. These constituents are illustrated in Figure 1.^[2–5]

It is generally agreed that, in hypoeutectoid steels, the presence of pearlite rather than proeutectoid ferrite is beneficial for increasing hardness/tensile strength but harmful to the toughness.^[1,7–9] In eutectoid/fully pearlitic steels, the yield strength has been reported to follow a Hall–Petch type of relationship with respect to the interlamellar spacing,^[1,10] which has been explained on the basis of a dislocation pile-up model.^[9,11]

In low-carbon steels, where pearlite coexists with ferrite in the microstructure, other pearlite features rather than interlamellar spacing would also affect the properties. For instance, the contribution of pearlite volume fraction to the strength is considered to obey the law of mixtures.^[7,10,12] The nodule and colony size would also contribute to the strength of this type of steels according to the Hall–Petch relation.^[1,13] It is also reported that the impact transition temperature decreases with a finer colony size.^[12] Ray and Mondal^[7] have also discussed that the strength of hypoeutectoid steels would be affected by the characteristics of proeutectoid ferrite. It is well known that the grain refinement of ferrite improves the strength and toughness at the same time.^[1,10]

In polycrystalline steels, pearlite formation is more likely to take place at the grain boundaries or at the junctions between several grains.^[14] In hypoeutectoid

H. TORKAMANI, SH. RAYGAN, and J. RASSIZADEHGHANI are with the School of Metallurgy and Materials Engineering, College of Engineering, University of Tehran, Tehran, 111554563, Iran. Contact e-mails: H.torkamani@ut.ac.ir, shraygan@ut.ac.ir C. GARCIA-MATEO and D. SAN-MARTIN are with the Materialia Research Group, National Center for Metallurgical Research (CENIM-CSIC), Avda Gregorio del Amo, 8, 28040, Madrid, Spain. Contact e-mail: dsm@cenim.csic.es Y. PALIZDAR is with the Materials and Energy Research Center, Karaj, 3177983634, Iran.

Manuscript submitted November 9, 2017.

Article published online July 9, 2018

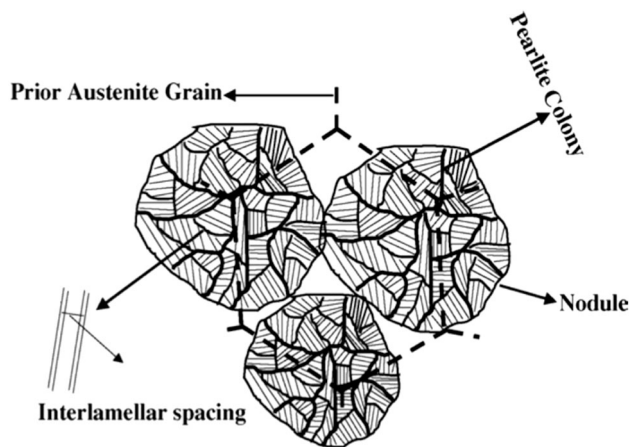


Fig. 1—Schematic illustration of the various constituents of pearlite.^[6] Reprinted from *Materials Science and Engineering A*, Vol. 404, A.M. Elwazri, P. Wanjara, and S. Yue. The effect of microstructural characteristics of pearlite on the mechanical properties of hypereutectoid steel, pp. 91-98, 2005, with permission from Elsevier.

steels, the proeutectoid ferrite nucleates first and, thus, the pearlite nucleation occurs at austenite-ferrite grain boundaries. Aranda *et al.*^[2] demonstrated that the Prior Austenite Grain Size (PAGS) is one of the most important factors affecting the pearlite morphology. The nodule and colony size are determined, not only by the PAGS, but also by the transformation temperature; the higher the transformation temperature and/or the coarser the PAGS, the larger they will be.^[2,15,16] With respect to the interlamellar spacing, for a given composition, it does not seem to be influenced by the PAGS and only by the atom diffusion kinetics at the transformation front which depends on the isothermal decomposition temperature below the eutectoid temperature (T_e).^[2,5,12,17-20] Zener^[21] provided the first theoretical model to predict the interlamellar spacing (σ) as a function of the undercooling and the rate-controlling mechanism (i) for carbon volume diffusion in the austenite ahead of the interface and (ii) for boundary diffusion through the interface between austenite and ferrite toward the cementite. In both cases, for a given chemical composition and using the maximum growth rate criterion, it can be found that this parameter (σ) is inversely proportional to the undercooling below T_e ; *i.e.*, the interlamellar spacing increases as the transformation temperature rises. According to this model, as discussed by Caballero *et al.*,^[22] it is found that $\sigma_{VD} > \sigma_{BD}$, where σ_{VD} and σ_{BD} are the interlamellar spacing predicted under the volume diffusion and boundary diffusion-controlled growth, respectively.

In alloyed steels, during pearlite growth, substitutional solute partitioning generally takes place between ferrite and cementite^[23] and, with the exception of cobalt, all substitutional alloying elements retard this transformation. As it has been discussed by Sharma *et al.*^[24] and by Tewari *et al.*,^[25] at low supersaturations (high transformation temperatures), partitioning of alloying elements is required thermodynamically and

the transformation is controlled by the boundary diffusion/partitioning of substitutional alloying elements. On the contrary, at high supersaturations (low transformation temperatures), partitioning becomes more difficult and the transformation may occur without significant partitioning and mainly controlled by carbon diffusion. Substitutional elements would influence the pearlite growth *via* affecting the carbon concentration gradients and the driving force at the transformation front because their diffusion coefficient is much lower than that of carbon and they require more time to partition. The influence of the main alloying elements like Mn, Cr, and Si has been extensively investigated in the literature.^[25-27] The steels under investigation have the particularity of the addition of RE (La and Ce in this research) to a reference Nb-microalloyed steel. These RE elements are known to have a large covalent atomic radius (0.1877 nm and 0.1825 nm, respectively) while that of Fe is 0.1210 nm. Accordingly, the diffusion of solute RE in Fe is slow and they would be expected to have a strong influence on diffusional transformations.^[28] Considering this difference in atomic radius, segregation of RE atoms to lattice defects would be also expected. Regarding the partitioning/segregation of RE elements during the pearlite growth, there exist contradictory surveys in the literature. Lu *et al.*^[29] have suggested that these elements would segregate on Fe_3C /ferrite interfaces where they dissolve more in ferrite (rather than in Fe_3C). In contrast, another publication reports that RE partition to Fe_3C at Fe_3C /ferrite interfaces which would cause more distortion of the cementite crystal lattice rather than ferrite. Consequently, the stronger effect of RE on the interplanar distance between Fe_3C layers has been detected.^[30]

Regarding the influence of RE on the morphology of pearlite, the effect of RE on the interlamellar spacing was investigated by Wang *et al.*^[31] They indicated that the RE in solid solution could reduce the thickness of Fe_3C ; however, such observations have not been argued in detail. Similarly, other researchers have declared that RE can reduce the pearlite lamellar distance in steels,^[29,30,32-34] but no clear discussion regarding the mechanisms involved has been carried out in these publications.

The majority of the works carried out on the use of RE in steels have focused on the inclusion modification and purification of steels. However, works concerning the effects of RE on the phase transformations and the product microstructures are scarce and contradictory. To the authors' knowledge, there have not been any significant detailed analysis of the pearlite microstructure in RE-added steels and the results obtained up-to-date are not well understood yet. Due to their importance for the steel-making sector and prospective impact on the mechanical properties, attentions should be focused on the potential ability of minor RE additions to refine the microstructure. Hence, in this study, attempts have been made to investigate and clarify the effects of RE addition on the pearlite microstructure in cast microalloyed steels.

Table I. Chemical Composition of the Base Steel (Fe to Balance)

Elements	C	Si	Mn	S	P	V	Nb	Mo	Cu	Al	Cr
Weight Percent	0.16	0.30	1.00	0.01	0.02	0.11	0.05	0.01	0.09	0.04	0.06

Table II. Results of ICP Technique Showing the Amount of RE in Studied Steels

Steels	Elements (ppm)				
	Ce	La	RE (La + Ce)	O	N
Base	< 10	< 10	—	96 ± 10	113 ± 4
RE-added	127.0	72.5	199.5	93 ± 6	112 ± 3

The content of O and N in the steels is also provided.

II. EXPERIMENTAL PROCEDURES

A. Steel Casting and Composition

A total of 100 kg of a clean low-carbon scrap steel was melted in an open air lined induction furnace. Alloying elements and carbon content were adjusted when the melt reached 1650 °C. Chemical composition of the melt (base steel) was measured onsite by Optical Emission Spectrometry (OES: ARL 3460) technique (Table I). The melt was deoxidized by Al shot in the furnace. A total of 7 g of a misch metal, containing 37.8 wt pct lanthanum (La) and 62.1 wt pct cerium (Ce), was placed in the bottom of a carrying ladle. Pouring the melt into the ladle ensured obtaining the same composition as the base steel but containing RE. Both of the molten alloys were cast into the sand molds. The amount of RE remained in the solidified steel was measured by Inductively Coupled Plasma (ICP: Optima 7300 DV) technique (Table II). In addition, the amount of O and N in the ingots was measured using a gas analyzing equipment (model: LECO TC-436 AR) (Table II). Microstructure of the as-cast materials were observed by Optical (OM: NIKON ECLIPSE LV150N) and Scanning Electron Microscopies (SEM, QUANTA 450) in order to monitor any possible influences of RE in the as-cast condition.

B. Heat Treatments

After the casting of the steels, since the microstructures were coarse and inhomogeneous, they were homogenized (1100 °C for 5 hours) and then normalized (950 °C for 30 minutes) in a muffle furnace (model: AZAR M11L) under the air atmosphere. The effect of RE on the microstructure (colony/nodule size of pearlite) of the normalized steels was subsequently investigated as described below in Section II-C.

In addition, as the interlamellar spacing of pearlite is dependent on the steel composition and applied heat treatment (*e.g.*, the cooling rate and the transformation temperature), dedicated isothermal experiments were carried out to investigate the influence of RE addition

on this parameter. With this aim, normalized samples (cylindrical samples of 10 mm in height and 4 mm in diameter) were heated at 5 °C/s up to 1050 °C, held for 10 minutes, quenched at 100 °C/s down to 650 °C, held for 15 minutes, and then quenched to room temperature. This heat treatment has been performed using the heating/cooling system of a high-resolution dilatometer (model: Bähr 805 A/D DIL Plastodilatometer) to accurately control the heat treatment schedule.

To ensure that the effect of RE addition on the interlamellar spacing is only attributed to its presence in solid solution and not to its indirect influence on the T_e , which determines the undercooling, the critical transformation temperature of both steels (with and without RE) during cooling (Ar₃) was experimentally determined by dilatometry. With this aim, the normalized samples with the same dimensions as described before were fully austenitized at 1050 °C in the dilatometer. Then, they were very slowly (0.05 °C/s) cooled down to a temperature (600 °C) at which the transformation is complete. This is the Cooling Rate (CR = 0.05 °C/s) normally regarded as quasi-equilibrium conditions.^[3,35] Finally, the samples were quenched (by fast cooling) from 600 °C to room temperature.

C. Microstructural Characterization

Prior to the inspection of the heat-treated samples under OM and SEM (models: Hitachi S 4800 J and QUANTA 450), they were prepared metallographically using the standard procedures. The samples were dry ground and then polished using a lubricant which was a mix of ethanol and DP-Lubricant Blue. Deep primary etching with Nital 2 pct solution was used to ensure that any effects introduced by polishing were removed. The samples were polished carefully with 1 μm diamond paste again and then lightly etched. This process was repeated twice. In the last preparation step, a light etch was given to the samples. This repeated polishing and etching procedure leads to an optimum disclosure of the morphology of pearlite in the microstructure as suggested by Capdevila and his coworkers.^[3]

Pearlite nodules were delineated using GIMP software (version 2.8) on several randomly selected OM images taken on the samples in normalized and as-cast conditions. The volume fraction and nodule size of pearlite in the normalized samples were measured on these processed micrographs by means of an image analyzing software (ImageJ, 1.47v). The same process was employed for measuring the ferrite grain size. Likewise, these parameters (size of pearlite nodules and ferrite grains) were also measured in the as-cast samples. The same method used for measuring the nodule size was employed on random SEM images to estimate the

pearlite colony size in the normalized samples, and the average has been reported. It should be mentioned that the standard errors of the reported results have been calculated according to ASTM E2586, which represents < 5 pct of the average value measured for each case. Considering the nodules and colonies of pearlite as circular shapes in 2D, their size (equivalent diameter, d) has been calculated from their average area (A) according to $d = 2\sqrt{A/\pi}$.

It is worth mentioning that the measurement of the pearlite colony/nodule size has been carried out on the base and RE-added samples taken from the same locations in the cast ingots so as to prevent any possible influences caused by casting condition.

As it was explained in the previous section, as a complement to the investigation carried out on normalized samples, which focuses on the influence of the RE on the colony/nodule size of pearlite, an isothermal experiment was carried out to investigate the influence of RE on the interlamellar spacing of pearlite. A transmission electron microscope (TEM, model JEOL JEM 3000F, acceleration voltage of 300 kV) equipped with an Energy Dispersive X-ray Spectrometer (EDS, Oxford INCA) has been used for the close observation of the pearlite structure as well as to detect any elemental segregation within the pearlite structure on these isothermally heat-treated samples. This microscope is in the ultrahigh-resolution configuration with a spatial point resolution of 0.17 nm under TEM mode. The EDS detector is capable of providing microanalysis data with a resolution of a few nanometers, enough to unveil the segregation of RE elements within the pearlite microstructure.^[36] For these observations, the samples were prepared from 3 mm in diameter disks, ground to ~ 80 μm in thickness, and then electropolished by Tenupol 5 using 95/5: acetic/perchloric acid electrolyte at room temperature and the voltage of 40 V.

To determine the interlamellar spacing of pearlite, the circular test grid method (also known as circle intercepts) has been employed. This methodology allows estimating the mean random interlamellar spacing, σ_r , and it is ideal for the determination of the mean true spacing, σ_t . This method guarantees orientation randomization and provides a constant test line length for each measuring field^[37–39] which are much more difficult to be satisfied when using a grid with straight test lines.^[38] This method has been successfully used by other researchers, in which a circular test grid of diameter d_c is superimposed on the pearlite lamellae.^[5,20,40,41] Then, the number, n , of intersections of carbides with the test circular line is counted. This procedure is repeated on a number of fields chosen without bias. If a single pearlite colony is cut by a test circle of diameter d_c (Figure 2), the mean random spacing σ_r is calculated from the following equation^[38]:

$$\sigma_r = \frac{\pi \cdot d_c}{n \cdot M}, \quad [1]$$

where M is the magnification and d_c/M can be considered as the actual size of the circle diameter appeared on the micrographs. For pearlite with a constant

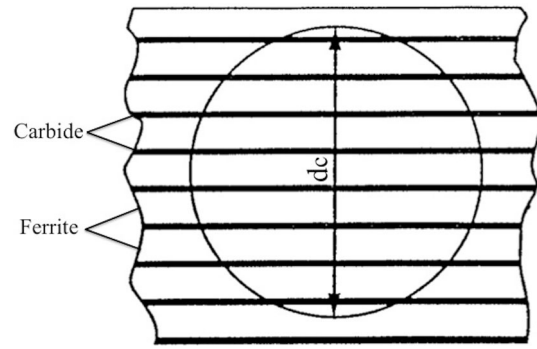


Fig. 2—Schematic illustration of a pearlite colony intersected by a circular test grid of diameter d_c .

spacing within each colony, the mean true spacing σ_t is related to the mean random spacing σ_r as follows^[38,39]:

$$\sigma_t = \frac{\sigma_r}{2}. \quad [2]$$

Finally, thermal etching experiments were also carried out to reveal the prior austenite grain boundaries and determine the PAGES after the austenitization heat treatments at 1050 °C, on the isothermally treated samples, according to the methodology used by San-Martin and his coworkers.^[42] This was carried out in the same high-resolution dilatometer as described in previous section (model: Bähr 805 A/D DIL Plastodilatometer) under high vacuum conditions and using cylindrical samples of the same dimensions. After delineating the grain boundaries of austenite revealed by this method on OM images (by the help of GIMP software), the average grain size was measured according to the procedure explained for measuring the pearlite nodule/colony size.

III. RESULTS

A. As-Cast Microstructure

Figure 3 shows OM and SEM images of the microstructure of both steels in the as-cast condition. In the OM images (Figures 3(a) and (b)), the solidified grains are marked with dash lines. These grains seem to be finer in the presence of RE. These images depict the characteristic microstructures that have been often observed in the as-cast condition. In a recent work of the authors^[43] carried out on this type of steels, it has been observed that the size of most of the solidified grains ranges from 250 to 400 μm in the base steel, while this value lies between 200 to 300 μm in RE-added steel. This would affect the fineness of the product phases upon cooling to room temperature. The current results of microstructural characterization in the as-cast condition suggest that the average size of pearlite nodules and ferrite grains are refined from around 14 to 10 μm and 18 to 13 μm by RE addition, respectively. The SEM images also show the distribution of pearlite in ferrite matrix of the base (Figure 3(c)) and RE-added

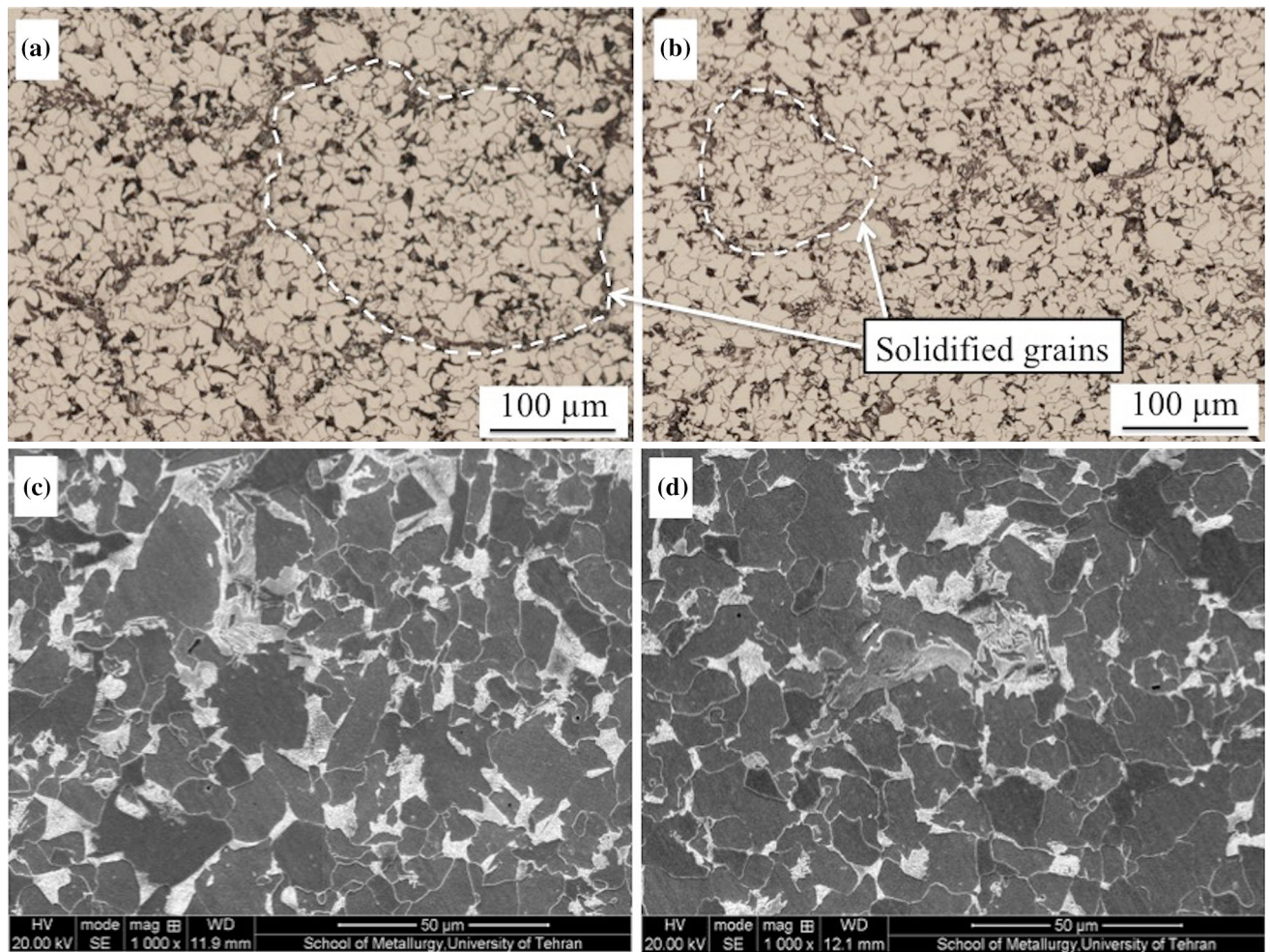


Fig. 3—OM images of microstructure of the as-cast (a) base and (b) RE-added steels along with the SEM micrographs illustrating the pearlite nodules in the matrix of the (c) base and (d) RE-added steel in the same condition.

(Figure 3(d)) steels. However, in these images (at higher magnification), the solidified grains are not as obvious as they appeared in the OM images (Figures 3(a) and (b)). It is worth mentioning that, since these casts have not experienced the homogenizing treatment, inhomogeneities may be present in their microstructure.

B. Normalized Microstructure: Nodule and Colony Size

In industry, the normalizing treatment is a conventional process applied to low-carbon steels to achieve their final properties. Figure 4 shows the microstructure of the normalized base and RE-added steels. It can be seen that the addition of RE led to finer microstructural components (Figure 4(b)) compared to the base steel (Figure 4(a)); distribution of the finer pearlite nodules can be observed in the matrix of RE-added steel. The volume fraction and nodule size of pearlite, as well as the ferrite grain size, were measured on at least 5 random OM images at a given magnification. The results of these measurements are summarized in Table III. It can be observed that the addition of 200 ppm of RE could effectively reduce the nodule size (~ 33 pct size reduction) and the ferrite grain size after

normalizing. However, it does not modify the pearlite/ferrite volume fractions, significantly.

Figure 5 shows two characteristic and representative SEM images of some selected nodules present in the microstructure of the base (a) and RE-added (b) steels. Although the images have been taken at different magnifications, Figure 5(a) shows a nodule composed of relatively large colonies in the microstructure of the base steel, while a smaller nodule consisting of the finer colonies can be found in the matrix of RE-added steel (Figure 5(b)). The colony size of pearlite in the normalized condition was measured for the base and RE-added steels following the procedure described in Section II-C; the results of this characterization are summarized in Table III.

C. Isothermally Transformed Pearlite: Interlamellar Spacing

Figure 6 depicts the relative change in length, as a function of the temperature, recorded during the complete cycle carried out to transform the microstructure isothermally, at 650 °C (15 minutes), after an austenitization heat treatment at 1050 °C (10 minutes) for the

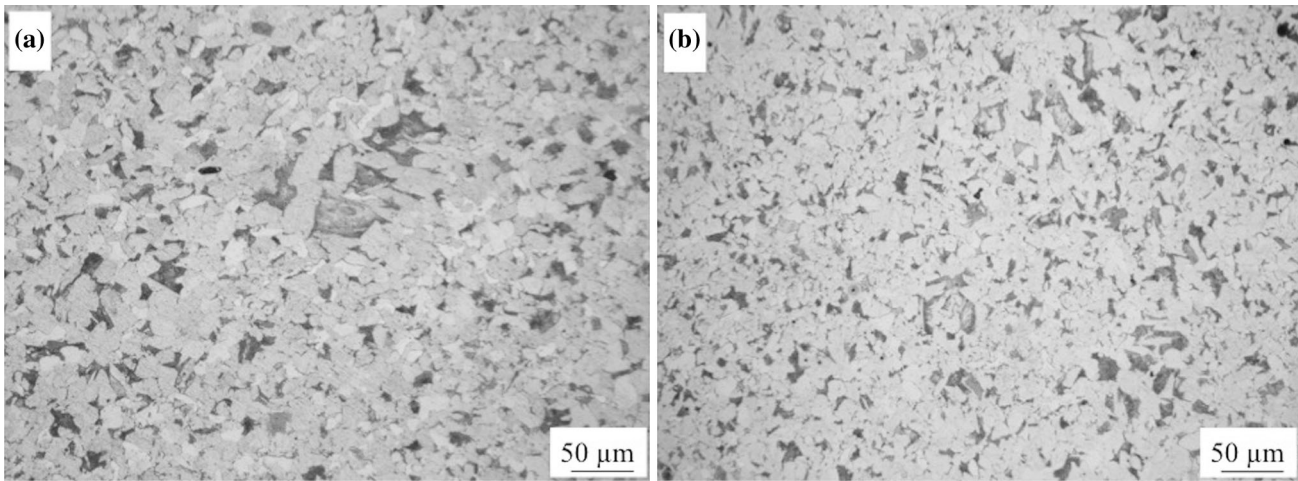


Fig. 4—OM images showing the microstructure of the normalized (a) base and (b) RE-added steels.

Table III. Microstructural Characteristics of the Normalized Samples

Steels	Pearlite Pct	Average of Pearlite Nodule Size (μm)	Average of Pearlite Colony Size (μm)	Average of Ferrite Grain Size (μm)
Base	23 ± 0.8	9 ± 0.4	5.3 ± 0.2	12 ± 0.6
RE-added	21 ± 0.9	6 ± 0.3	3.4 ± 0.2	7 ± 0.4

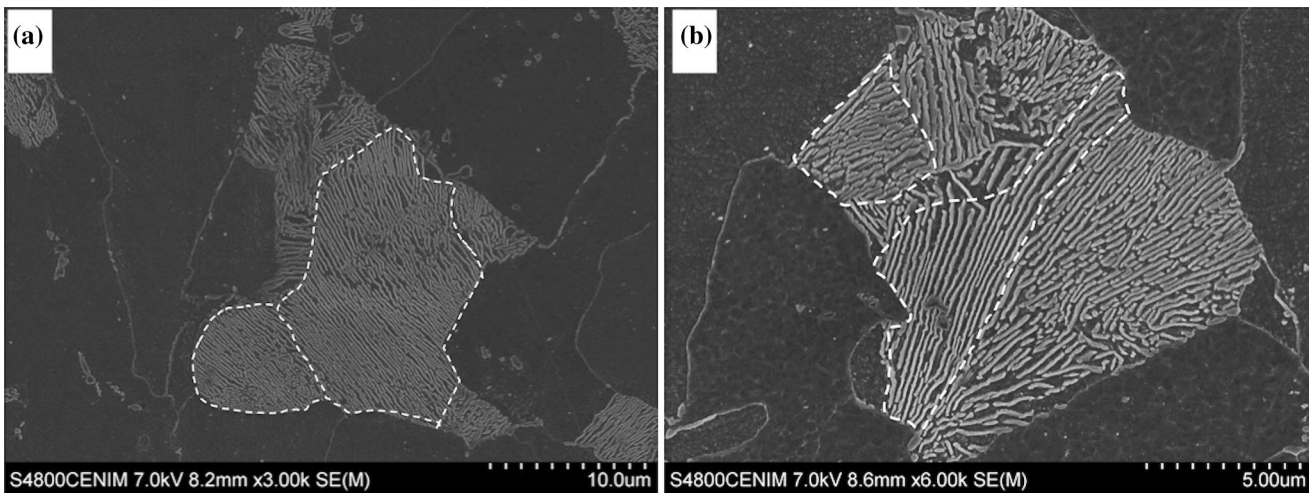


Fig. 5—SEM images of characteristic pearlite nodules in the base (a) and RE-added (b) steels. Some colony borders inside of a nodule (a colony contains lamellae with the same orientation) have been highlighted using white dash lines.

base (black solid line) and RE-added (red dash line) steels. In both steels, during heating at $5\text{ }^{\circ}\text{C/s}$, the initial ferrite + pearlite microstructure (see Figure 4) expands quasi-linearly up to a temperature ($\sim 750\text{ }^{\circ}\text{C}$) where a two-step contraction is observed; the first small contraction is related to the pearlite-to-austenite transformation followed by the ferrite-to-austenite transformation.^[44] Once the microstructure is fully austenitic, the steel continues expanding linearly. Fast cooling after the austenitization has ended in a linear contraction down to the isothermal targeted

temperature ($650\text{ }^{\circ}\text{C}$), at which a pronounced expansion of the sample has been observed for both steels. During the final quenching after the isothermal step, the sample proceeds again in a quasi-linear way; the lack of an expansion reveals the absence of bainite/martensite formation during cooling. Thus, this implies that the microstructure has been fully transformed to ferrite + pearlite during the isothermal step.

Figure 7 shows characteristic SEM images corresponding to the microstructure of the isothermally heat-treated samples. These microstructures consist of

pearlite nodules in a ferrite matrix. It can be seen that, compared to the base steel (Figure 7(a)), the microstructure of RE-added steel (Figure 7(b)) contains finer ferrite grains as well as finer pearlite nodules.

Figure 8 illustrates how the interlamellar spacing has been determined using SEM images. These micrographs show characteristic and representative lamellae structures found in each steel. As it was described in Section II-C, a typical test grid has been superimposed on the pearlite lamellae in both studied steels and the number of intersections has been counted. The results of the average of true interlamellar spacing calculated according to Eqs. [2] and [3] are given in Table IV. Comparing the interlamellar spacing of pearlite in the base steel (Figure 8(a)) with the one measured for RE-added steel (Figure 8(b)), it has been found that RE addition reduces this parameter significantly (~ 25 pct). As it has been mentioned before, this procedure has been repeated on randomly selected fields embracing

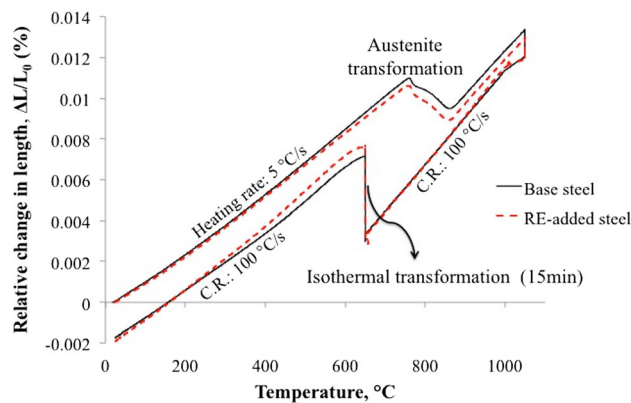


Fig. 6—Relative change in length recorded during the complete cycle carried out to transform the microstructure isothermally at 650 °C after an austenitization heat treatment at 1050 °C for 10 min.

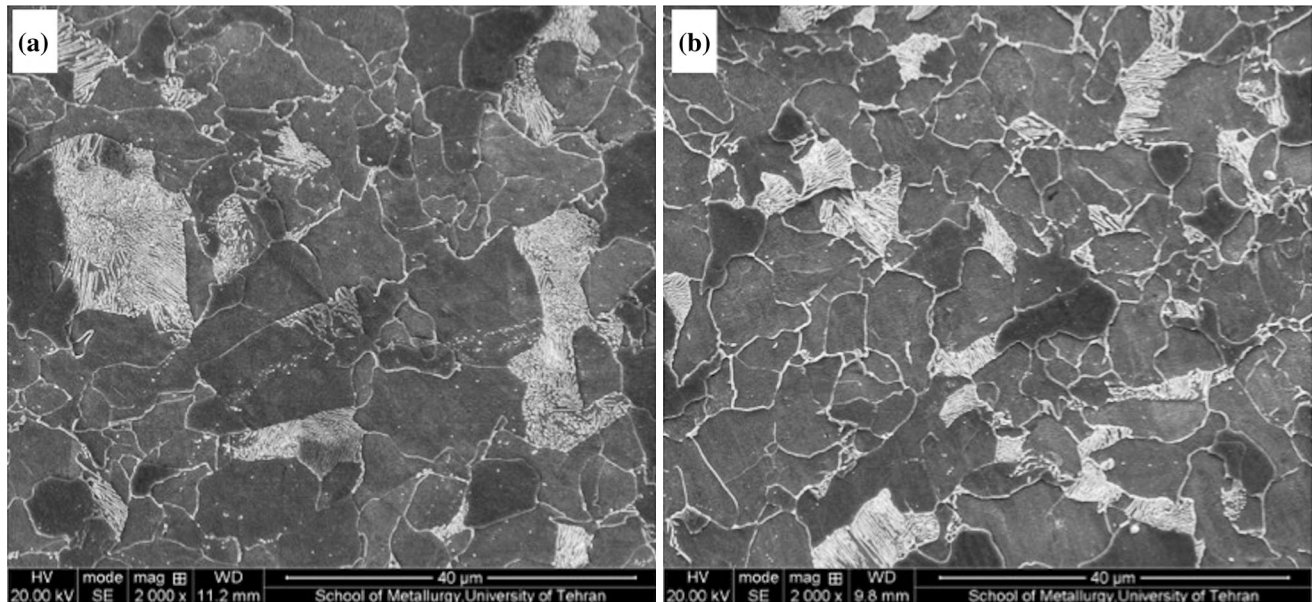


Fig. 7—SEM micrographs of the isothermally heat-treated (a) base and (b) RE-added steels.

sound pearlite lamellae until reaching an accurate measurement. It is noteworthy that the circle should not overlap different pearlite colonies or cover the ferrite grains as it should be drawn on a colony with the same orientation of lamellae.

IV. DISCUSSION

A. Effects of RE on the Pearlite Microstructure in the As-Cast and Normalized Samples

The structure of low-carbon steels, which experience the peritectic transformation, is strongly dependent on the number of solidification nucleation sites.^[45] Non-metallic inclusions that appear in various stages of the solidification of steels may act as the cores for the heterogeneous nucleation to refine the solidification structure and/or may inhibit grain growth by Zener pinning in the solid state.^[31,46–49] In this regard, it has been reported that RE form non-metallic inclusions in the molten steel that serve as heterogeneous nucleation sites during solidification.^[50–53] The role of RE particles as potent nucleation sites during solidification has been verified in a recent work of the authors,^[43] in which a finer solidified structure and, consequently, a finer cast structure has been obtained in the RE-added steel at room temperature. This is observed in the optical and SEM micrographs provided in Figure 3. Besides, after the normalization heat treatment at 1050 °C, the OM images and the results of pearlite characterization (Table III) show that the RE-added steel possesses a finer-grained microstructure compared to the base steel. This is mainly attributed to the fact that the normalized microstructure of RE-added steel inherits the finer as-cast microstructure. It would be also expected that fine RE inclusions have assisted the refinement of the microstructure due to the pinning effect on the prior

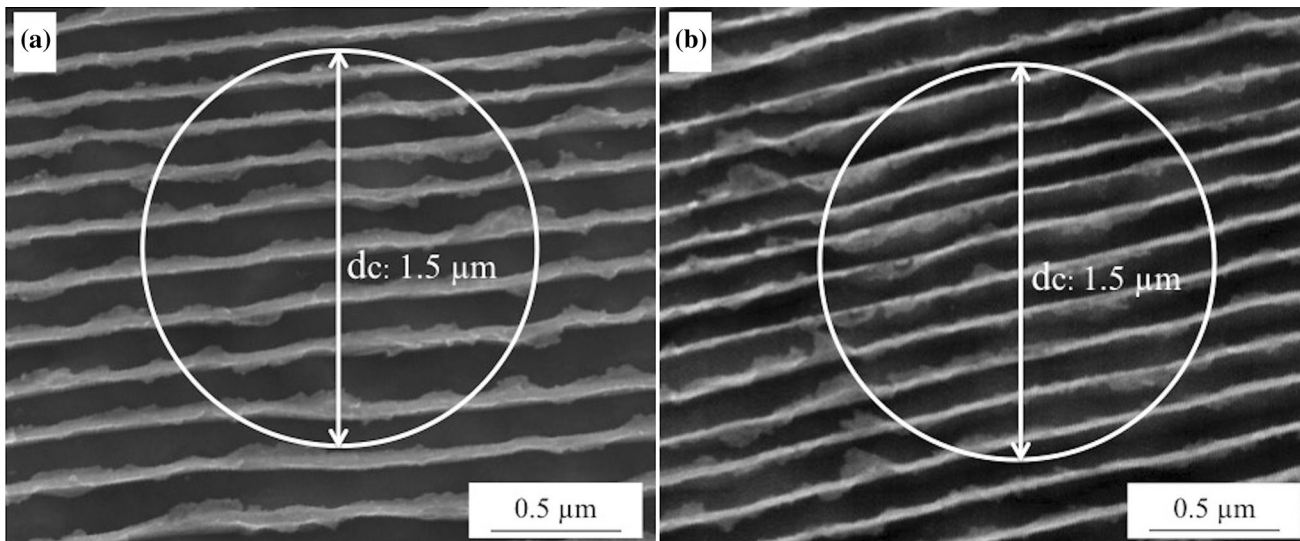


Fig. 8—SEM images illustrating the test grid on the pearlite lamellae in the (a) base and (b) RE-added steels.

Table IV. The Results of Interlamellar Spacing Measurement

Steels	Average of the True Interlamellar Spacing (μm)
Base	0.152 ± 0.01
RE-added	0.115 ± 0.01

austenite grain boundaries during the heat treatments, leading to smaller austenite grain size in RE-added steel. It has been reported that the efficiency of inclusions in the boundary pinning is related to the volume fraction and size of the inclusions.^[54,55] Thus, during the heat treatments, inclusions with different sizes would act differently when meeting a passing boundary. However, to take advantage of this effect, the boundaries should intersect the inclusion particles in order to prevent grain growth at that elevated temperature. Aforesaid effects, in turn, would result in a refined ferrite+pearlite microstructure in the RE-added steel upon cooling to room temperature.^[48,49,56] In the following paragraph, this consecutive incident is further explained.

As it has been discussed in the introduction of this paper, it is well known that the nucleation rate of pearlite is very structure sensitive as its nucleation occurs readily at grain boundaries.^[14] In the case of the hypoeutectoid low-carbon steels, the earlier formation of proeutectoid ferrite rejects carbon from this phase and enriches the untransformed austenite. Ferrite-austenite interfaces would serve as nucleation sites for the formation of pearlitic cementite, from which pearlite growth would begin.^[2] A finer austenitic microstructure (higher number density of grain boundaries compared to coarser microstructures) would stimulate the nucleation of a higher population of proeutectoid ferrite grains. Thus, the smaller untransformed carbon-enriched austenite areas lead to smaller transformed pearlite nodules (compared to coarser austenitic microstructures). This is the case of the

RE-added steel compared to the base steel. The consequences of this scenario can be seen in Figure 9 where representative and finer pearlite nodules are shown in the microstructure of normalized RE-added steel.

Aranda *et al.*^[2] reported that abrupt changes in the PAGS modify the total pearlite volume fraction formed in the final microstructure. They observed that a change in the PAGS from 5 to 120 μm would increase the volume fraction from ~ 0.6 to ~ 0.9 and explained that a finer PAGS would increase the number of nucleation sites available for the transformation of austenite to proeutectoid ferrite. This would, thus, enhance the formation of ferrite, which in turn would result in a lower volume fraction of the pearlite. A similar argument and results have been discussed by Liu *et al.*^[57] who also showed experimentally that the transformation temperature would determine how the variation in the PAGS affects the volume fraction of ferrite or pearlite; the higher the isothermal temperature, the weaker this effect would be. Although these investigations deal with the isothermal transformation, their findings still give a helpful insight into the explanation of the current results. It should be mentioned that, in the current study, the transformation temperatures determined by the continuous path did not modify the phase fractions of ferrite/pearlite obtained in the normalized steels because these steels experienced the same cooling process (air-cooling) from austenitization temperature and proeutectoid ferrite/pearlite have conceivably formed through a similar temperature range in the both studied steels. Although the PAGS could not be directly measured in these normalized samples, according to these reports, one could anticipate that RE would indirectly modify the phase fractions by changing the PAGS. The differences observed in the ferrite grain size and pearlite nodule/colony size suggest that the PAGS was not so different as compared to those previous works reported above and, while affecting the microstructural features of ferrite/pearlite (Table III), they would not affect the phase fractions significantly.

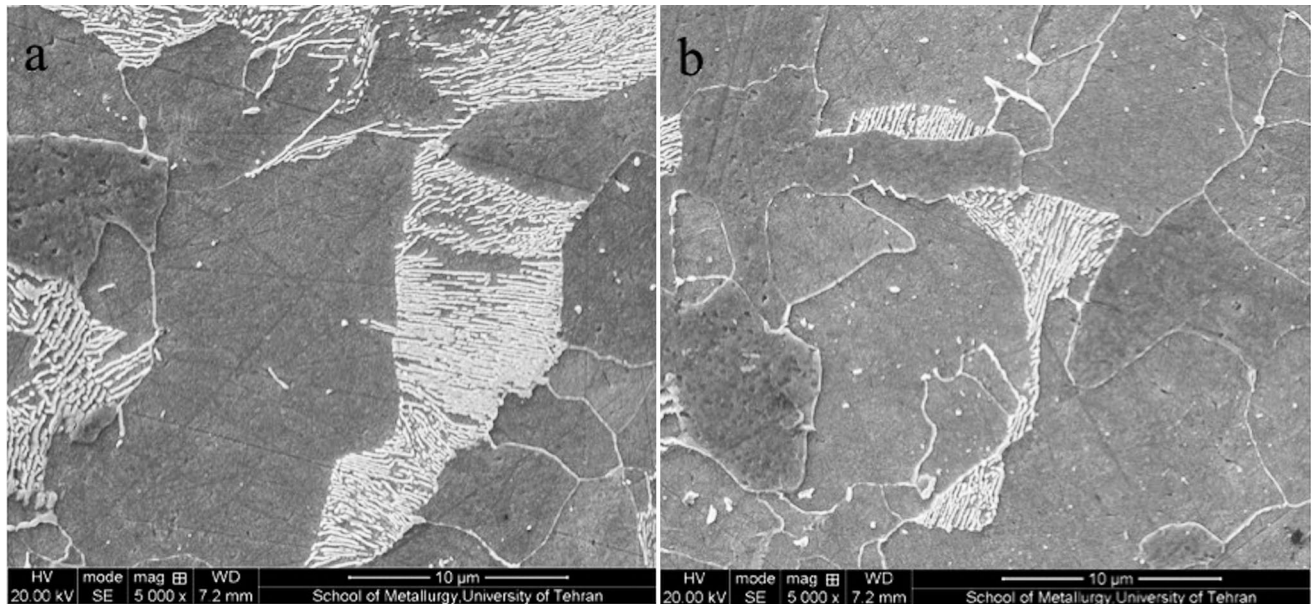


Fig. 9—SEM images consisting of (a) relatively coarse pearlite nodules distributed in the coarse ferrite matrix in the base steel and (b) fine pearlite nodules nucleated on the ferrite boundaries in the normalized RE-added steel.

B. Effects of RE Addition on Isothermally Transformed Pearlite: The Interlamellar Spacing

The dilatometry results in Figure 6 have shown that, after the austenitization at 1050 °C (10 minutes), during the isothermal heat treatment at 650 °C (15 minutes) the microstructure has fully transformed to a mixture of ferrite and pearlite and no bainite/martensite has been detected in the dilatometry plot after quenching to room temperature. This has been confirmed by the SEM images presented in Figure 7. As for the normalized samples (Figure 9), these images show that the microstructure (both the ferrite grain size and the pearlite nodules) is finer in the RE-added steel. In this case, the prior austenite grain boundaries have been revealed by the thermal etching method and the grain size was measured by image analysis for the temperature of 1050 °C (10 minutes) prior to the isothermal step. The results of this characterization conclude that the RE-added and base steels have an average austenite grain size of $13 \pm 1 \mu\text{m}$ and $21 \pm 1 \mu\text{m}$, respectively. Apart from the influence of RE on the refinement of the cast structure, already discussed in the previous section for the normalized samples, the Zener pinning effect of fine inclusions on grain boundaries can be considered as another probable cause of this refinement in RE-added steels during the heat treatments.^[54,55] It is well known that the finer the austenite grain size, the finer the product phases will be upon cooling to room temperature.^[58]

The results concerned with the measurement of the interlamellar spacing of pearlite isothermally transformed at 650 °C (Table IV) indicate that the RE-added steel has a significantly smaller interlamellar spacing than the base steel. It was stated above that, when the austenite transforms isothermally to pearlite, any changes in the interlamellar spacing of

pearlite depends solely on the alloy composition.^[3,17,21,59,60] For the same steel composition, the larger the undercooling, the higher the free energy change accompanying the transformation would be. However, since the reaction is diffusion controlled, the atomic diffusion distance reduces due to the decrease in the diffusivity. As a consequence, the interlamellar spacing decreases. In a similar fashion, under continuous cooling conditions, the interlamellar spacing would depend on the cooling rate and the alloy composition. Faster cooling rates would promote the transformation at lower temperatures (larger undercooling) leading to a refinement of the interlamellar spacing.^[40]

It should be noted that, apart from the effects of solute RE, the added amount (200 ppm) of these elements inhibits the formation of MnS in such a steel.^[53] As a result, it is expected that more Mn would be in solid solution, which may affect the T_c and, consequently, the undercooling for the studied steel. Assuming that all the solute S (0.01 wt pct) would react with Mn in order to form MnS, based on the chemical composition of the studied steels and atomic mass of these elements, about 0.017 wt pct of Mn would be required to consume the entire S. Therefore, the inhibition of MnS formation by RE addition would release a maximum of 0.017 wt pct Mn as solid solution in the RE-added steel. According to Eq. [3] given by Reardon,^[61] the critical transformation temperature A_1 would decrease less than 1 °C as a result of this increase in Mn in solid solution. Moreover, it has been reported that this element would have a negative effect on the refinement of lamellar spacing.^[61–63] Thus, compared to the base steel, the potential effect of this minor increase in Mn on the refinement of the interlamellar spacing can be discarded.

$$A_I (^{\circ}\text{C}) = 723 - 10.7 (\% \text{Mn}) - 16.9 (\% \text{Ni}) + 290 (\% \text{As}) + 29.1 (\% \text{Si}) + 16.9 (\% \text{Cr}) + 6.4 (\% \text{W}).$$

[3]

However, to investigate further the influence of these variations in Mn and RE on the T_e and, thus, on the undercooling, dilatometry tests have been carried out on the normalized samples according to the heat treatment schedule described in Section II-B. It is generally considered that the transformation temperatures (A_{r3} , A_{r1}) obtained after cooling at rates as slow as 0.05 °C/s are close to those met under equilibrium,^[3,35,64] the reason why this cooling rate is used as an empirical approximation to determine transformation temperatures. Figure 10 shows the dilatometry results for the base and RE-added steels. Only the relative change in length, $\Delta L/L_0$, undergone by the samples during cooling after the austenitization heating cycle, is shown in Figure 10(a). In Figure 10(b), the temperature range (850 °C to 600 °C), where the expansion has been observed, has been highlighted; the expansion is due to the austenite-to-ferrite and austenite-to-pearlite transformations. In this graph both, $\Delta L/L_0$, and its derivative, $d(\Delta L/L_0)/dT$, have been represented together for both curves (RE-added steel curves in dash lines). The expansion undergone by the samples during heating is very similar to that presented in Figure 6, the reason why it has not been shown in this figure. From the comparison of these two plots, it can be concluded that the transformation behavior for both steels is very similar. During slow cooling, the samples contract linearly down to a temperature (A_{r3}) at which they start to expand due to the onset of the austenite-to-ferrite transformation. The A_{r3} estimated from these dilatometry plots are 790 °C and 791 °C for the base and RE-added steels, respectively. As the cooling

continues, there is a temperature at which a weaker expansion takes place due to the austenite-to-pearlite transformation. From the derivative plots, it could be suggested that the peak transformation rate is slightly lower for the RE-added steel. The austenite-to-pearlite transformation is considered to start at the inflection point that sets the transition between both transformations (this temperature corresponds to the peak in the derivative). It should be bear in mind that, as pearlite may nucleate in some regions of the microstructure where the driving force is high enough, while ferrite is still transforming in other regions, a small overlapping between both transformations may be expected. Nonetheless, this approach provides a reasonable estimate for the A_{r1} critical transformation temperature under quasi-equilibrium conditions. The A_{r1} values estimated from the dilatometry plots are 680 °C and 682 °C for the base and RE-added steels, respectively. The temperature at which the transformation is finished under slow cooling conditions is the same for both steels.

The results presented in Figure 10 and discussed above show that there are no differences in the T_e of both steels and, thus, the undercooling (driving force for pearlite nucleation) at the isothermal transformation temperature under investigation (650 °C) may be regarded as identical for both steels. In addition, it should be also pointed out that, contrary to its effect on the nodule and colony size, the austenite grain size does not affect the interlamellar spacing of pearlite.^[2] Hence, it could be suggested that in the steels under investigation, any changes in the interlamellar spacing will be correlated to how the elements in solid solution determine the carbon diffusion and the rate of the transformation. In this sense, the presence of RE in solid solution might be expected to play an important role.

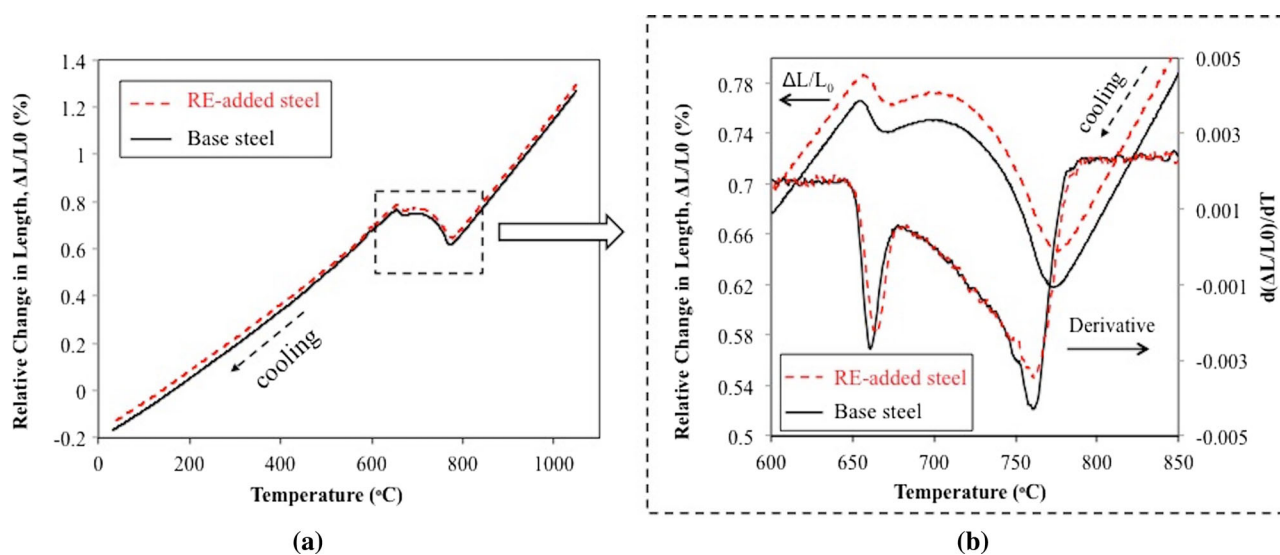


Fig. 10—(a) Temperature evolution of the relative change in length ($\Delta L/L_0$) during continuous cooling after austenitization at 1050 °C (10 min). The cooling was carried out in two steps: (1) at 0.05 °C/s down to 600 °C; (2) Quench (100 °C/s) from 600 °C to room temperature; and (b) $\Delta L/L_0$ and its temperature derivative are represented in the temperature range of 600 °C to 850 °C to undertake a more detailed analysis of the transformation behavior.

In pearlite, cementite is rich in carbon whereas ferrite accommodates very little carbon. Therefore, carbon needs to be redistributed between these two phases at the transformation front during the growth of pearlite. In this sense, as it was discussed in the introduction, the rate-controlling mechanism that operates (boundary/volume diffusion) will influence the interlamellar spacing. This parameter is notably affected by how the carbon diffusion is altered by the temperature and alloy composition.^[21, 65] A limited number of references can be found in the literature concerned with the effect of RE on the pearlite growth and its interlamellar spacing, while the influence of other alloying elements like Cr, Mn, Si, or Al on the pearlitic transformation has been the subject of several investigations so far.^[63,66,67] These findings can help to understand the potential role of solute RE on the refinement of the interlamellar spacing. For instance, Honjo *et al.*^[67] investigated the effects of Cr on the interlamellar spacing. They discussed that the refinement due to Cr in solid solution would be similar to that caused by the decrease in temperature, *i.e.*, it slows down carbon diffusion which, in turn, would reduce the diffusion distance during the transformation and, thus, the interlamellar spacing. In the case study under investigation, since the interaction coefficient of RE element and carbon is negative,^[33,68] it would likely decrease the diffusion coefficient of carbon, affecting the interlamellar spacing similarly to Cr.

When substitutional elements are present in steels, there are two principal mechanisms cited in the literature to explain the kinetics of pearlite growth, one involves the volume diffusion of carbon ahead of the transformation front, while the other relies on interfacial diffusion as the rate-controlling step. In fact, austenite-to-pearlite transformation can take place in two ways: (i) the alloying elements are partitioned between the parent (austenite) and product phases, and (ii) the alloying elements undergo no long range diffusion and the ratio of the alloying elements to iron remains the same in the product phases as in the parent phase. The latter reaction is then controlled by the diffusion of carbon.^[24] Determining which mechanism will control the growth of pearlite is mainly dependent on the transformation temperature below T_e . It is generally agreed that during the pearlite growth, alloying elements partition between the ferrite and cementite at low supersaturations (high transformation temperatures) and the growth is mainly controlled by alloying element boundary diffusion, while at high supersaturations (low transformation temperatures) pearlite growth occurs without a significant partitioning of the alloying element and is mainly controlled by carbon volume diffusion.^[21,25,59,60]

For the case in which growth is controlled by substitutional alloying elements, the transformation requires the local equilibrium redistribution of the alloying elements; thus, the reaction is slowed down considerably because of the relatively slow diffusion of the alloying element involved.^[24] Al-Salman *et al.*^[69]

investigated the segregation of the substitutional solute which was found to be kinetically feasible during the austenite-to-pearlite transformation. They argued that the redistribution/segregation of substitutional alloying elements could affect the growth of pearlite and its interlamellar spacing. In the current study, based on the high transformation temperature investigated (650 °C) which is close to the T_e measured experimentally ($Ar_1 \sim 680$ °C to 682 °C), the growth of pearlite would occur under the low supersaturation conditions (due to the low undercooling) and, thus, it would be controlled by substitutional alloying element diffusion. This growth mode is known as Partial Local Equilibrium (PLE).^[70,71] Partitioning of these substitutional elements requires more time as they diffuse much slower than carbon and may also influence its diffusivity.^[72] As it has already been discussed, under these conditions previous works have shown that the partitioning of substitutional alloying elements like Cr would take place. It would be expected that the partitioning of RE would also contribute to slowing down the transformation and decrease the interlamellar spacing of pearlite in a similar way as Cr. In this sense, Figure 11 shows TEM images depicting a pearlite interlamellar structure of a RE-added steel sample. The results of the line scan microanalysis show that Ce and La segregate inhomogeneously and mainly along the interfaces between ferrite and cementite within pearlite; the intensity peaks of RE (especially La) sharply rise at the interface of ferrite and cementite lamellae. This is not surprising because, due to the much larger radius of RE than that of Fe, they tend to segregate at the interface of ferrite/cementite as a result of the partitioning during pearlite growth.^[32] These interfaces are considered as the optimum paths for carbon diffusion during the transformation^[33]; it has been reported that the hindering of these carbon diffusion paths and the decrease in the carbon diffusion coefficient would influence the growth rate and refinement of the interlamellar spacing of pearlite.^[33]

It is noteworthy that, in Figure 11, the pattern of La and its segregation on the interface is clearer/sharper than that of Ce, while the amount of Ce in the investigated steel is higher than that of La (Table II). It could be due to the fact that diffusion of Ce is slower than that of La which originates from the larger migration energy and small solute-vacancy interaction of Ce.^[73] Moreover, it is worth mentioning that the diffusion coefficient of La, itself, is almost one order of magnitude lower than that of Fe self-diffusion.^[73]

One can conclude that the RE addition would refine the interlamellar spacing of the isothermally transformed pearlite according to the following possible contributions: (i) RE have a negative interaction coefficient with C which would decrease the diffusion coefficient of carbon, (ii) RE themselves need to redistribute between the phases and it is found that they tend to segregate mainly on the lamellae interface, and (iii) they would hinder the diffusion path for carbon. All these proposed mechanisms would slow down the

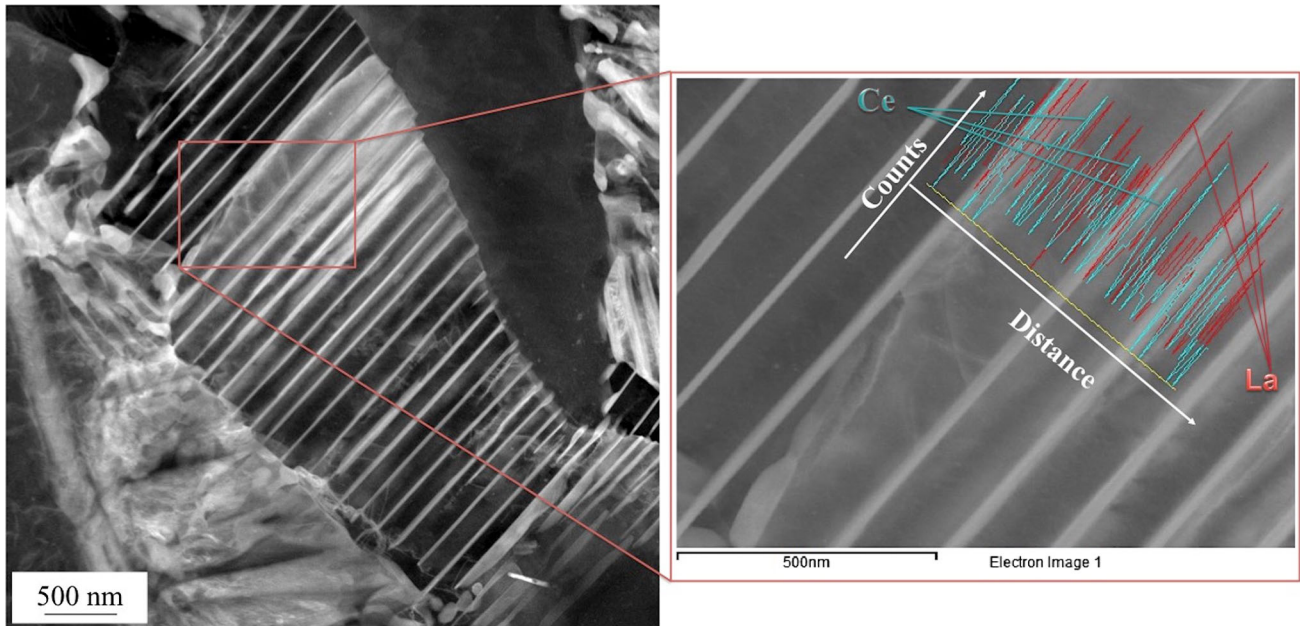


Fig. 11—TEM micrograph illustrating pearlite lamellae along with the results of the line scan microanalysis in RE-added steel.

diffusional processes, and thus, the spacing (diffusion step/distance) should be shortened in order to compensate the decrease in diffusion rate.

Apart from the factors already discussed above, the interfacial free energy associated with ferrite-Fe₃C interface (transformed from parent austenite) is another possible factor that affects the growth of pearlite. The interfacial energy gives rise to the capillarity effect, which in turn would affect the shape of ferrite and cementite tips (curvature term) at the advancing interface, changing the free energy curves of the phases and eventually the local equilibrium carbon concentration.^[74] In some studies, the capillarity effect has been considered as negligible,^[75,76] while, elsewhere, an approximate capillarity correction in free energy change and kinetic of the transformation has been taken into consideration^[77,78]; in the latter reports, researches claimed that the ignorance of the capillarity effect would change the kinetic and/or energy of the pearlite transformation which in turn would affect the pearlite interlamellar spacing. Sundquist^[79] has also suggested that the effect of capillarity should be considered on the growth of the pearlite formation, while the effect of a small concentration of alloying elements on the capillarity effect has been neglected. In that study, it has been indicated that the experimental results obtained are consistent with the model proposed. In the current study, this effect can be presumed not to be negligible but to be similar in the both steels under investigation. This assumption seems to be reasonable unless microalloying with 200 ppm of RE (part of which is present as solid solution) would be able to significantly alter the interfacial energy and consequently the capillarity effect. Regarding the influence of RE on the interfacial energy within the pearlite lamella, the experimental data suffer from the lack of evidences in literature; thus, this effect

of RE addition on the lamellar spacing remains open to question.

V. CONCLUSION

The results of this study allow us to conclude that the addition of RE to low-carbon microalloyed steels could affect the pearlite structure as summarized below:

1. Results of the microstructural examination by OM and SEM showed that RE are able to refine the cast structure in the studied steel, which is likely due to their role in providing nucleation sites that promote the solidification.
2. The refinement of the microstructure obtained by RE addition was observed in normalized samples as well; RE change the nodule and colony size of pearlite from 9 and 5.3 μm to 6 and 3.4 μm , respectively. However, it did not have a significant effect on the volume fraction of pearlite.
3. The interlamellar spacing of isothermally transformed pearlite was measured by the circle intercepts method and it was found that RE addition could refine this spacing from 0.152 to 0.115 μm . Because, except for the RE content, all the affective parameters (other alloying elements, transformation temperature and corresponding undercooling) were kept similar, the refinement of the spacing would be attributed to the presence of RE.
4. The results of TEM observations suggest that RE (La and Ce) segregate to the interface of ferrite and cementite within the pearlite structure during the pearlite growth, slowing down the diffusion of carbon. In addition, the reported negative interaction coefficient of RE with C would decrease the

diffusion coefficient of C. These influences of RE lead to having a smaller interlamellar spacing in the RE-added steel under investigation.

ACKNOWLEDGMENTS

The authors from the University of Tehran gratefully acknowledge the financial support provided by the Office of International Affairs and the Office of Research Affairs, College of Engineering, for the project number 8107009.6.34. The authors from CEN-IM-CSIC would like to acknowledge the financial support from Comunidad de Madrid through DIM-MAT-CM_S2013/MIT-2775 Project. The authors are grateful to the Phase Transformations and Microscopy labs from CENIM-CSIC. Mr. Javier Vara Miñambres from the Phase Transformations lab (CENIM-CSIC) is gratefully acknowledged for his continuous experimental support. The authors also acknowledge ICTS-Centro Nacional de Microscopía Electrónica (CNME) and Mr. Esteban Urones Garrote for the experimental supports in TEM lab.

REFERENCES

1. B. L. Bramfitt: in *Materials Selection and Design, ASM Handbook*, J. R. Davis, ed., ASM International, Ohio, 1998, pp. 153–73.
2. M.M. Aranda, B. Kim, R. Rementeria, C. Capdevila, and C. García de Andrés: *Metall. Mater. Trans. A*, 2014, vol. 45A, pp. 1778–86.
3. C. Capdevila, F.G. Caballero, and C. García de Andrés: *Acta Mater.*, 2002, vol. 50, pp. 4629–41.
4. F.P.L. Kavishe and T.J. Baker: *Mater. Sci. Technol.*, 1986, vol. 2, pp. 816–22.
5. F.G. Caballero, C. Capdevila, and C. Garcia de Andres: *Scripta Mater.*, 2000, vol. 42, pp. 537–42.
6. A.M. Elwazri, P. Wanjara, and S. Yue: *Mater. Sci. Eng. A*, 2005, vol. 404, pp. 91–98.
7. K.K. Ray and D. Mondal: *Acta Metall. Mater.*, 1991, vol. 39, pp. 2201–08.
8. B. Chokkalingam, S.S. Mohamed Nazirudeen, and S.S. Ramakrishnan: *Mater. Tehnol.*, 2011, vol. 45, pp. 159–62.
9. K. Nakase and I.M. Bernstein: *Metall. Trans. A*, 1988, vol. 19A, pp. 2819–29.
10. O.P. Modi, N. Deshmukh, D.P. Mondal, A.K. Jha, A.H. Yegneswaran, and H.K. Khaira: *Mater. Charact.*, 2001, vol. 46, pp. 347–52.
11. J.C.M. Li and Y.T. Chou: *Metall. Mater. Trans. B*, 1970, vol. 1B, pp. 1145–59.
12. B. Garbarz and F.B. Pickering: *Mater. Sci. Technol.*, 1988, vol. 4, pp. 328–34.
13. Y. Liang, Z.Y. Shi, and Y.L. Liang: *Adv Mater. Res.*, 2013, vols. 734–737, pp. 1531–35.
14. R.E. Smallman and R.J. Bishop: *Modern Physical Metallurgy and Materials Engineering*, 6th ed., Butterworth-Heinemann, Oxford, 1999, pp. 259–96.
15. A.R. Marder and B.L. Bramfitt: *Metall. Trans. A*, 1975, vol. 6A, pp. 2009–14.
16. A.R. Marder and B.L. Bramfitt: *Metall. Trans. A*, 1976, vol. 7A, pp. 365–72.
17. N. Ridley: *Metall. Trans. A*, 1984, vol. 15A, pp. 1019–36.
18. A.M. Elwazri, P. Wanjara, and S. Yue: *Mater. Charact.*, 2005, vol. 54, pp. 473–78.
19. J. Toribio, B. González, J.-C. Matos, and F.-J. Ayaso: *Metals*, 2016, vol. 6, pp. 1–12.
20. M. Wang, F. Zhang, and Z. Yang: *Mater. Sci. Technol.*, 2017, vol. 79, pp. 1–8.
21. C. Zener: *Trans. AIME*, 1946, vol. 167, pp. 550–95.
22. F.G. Caballero, C. Capdevila, and C. García de Andrés: *Mater. Sci. Technol.*, 2001, vol. 17, pp. 686–92.
23. H. Bhadeshia and R. Honeycombe: *Steels: Microstructure and Properties*, Butterworth-Heinemann, Oxford, 2017, pp. 101–34.
24. R.C. Sharma, G.R. Purdy, and J.S. Kirkaldy: *Metall. Trans. A*, 1979, vol. 10A, pp. 1129–39.
25. S.K. Tewari and C.R. Sharma: *Metall. Trans. A*, 1985, vol. 16A, pp. 597–603.
26. J. Fridberg and M. Hillert: *Acta Metall.*, 1970, vol. 18, pp. 1253–60.
27. C.R. Hutchinson, R.E. Hackenberg, and G.J. Shiflet: *Acta Mater.*, 2004, vol. 52, pp. 3565–85.
28. H.L. Liu, C.J. Liu, and M.F. Jiang: *Mater. Des.*, 2012, vol. 33, pp. 306–12.
29. W. Lu, H. Liu, T.Y. Hsu, and Z. Xu: *Scripta Metall. Mater.*, 1993, vol. 29, pp. 273–74.
30. L. Wang, Q. Lin, J. Ji, and D. Lan: *J. Alloys Compd.*, 2006, vols. 408–412, pp. 384–86.
31. L.M. Wang, Q. Lin, L.J. Yue, L. Liu, F. Guo, and F.M. Wang: *J. Alloys Compd.*, 2008, vol. 451, pp. 534–37.
32. T.Y. Hsu: *SIJ Int.*, 1998, vol. 38, pp. 1153–64.
33. C.J. Liu, Y.H. Huang, and M.F. Jiang: *Adv. Mater. Res.*, 2011, vols. 194–196, pp. 137–242.
34. C. Liu, Y. Huang, and M. Jiang: *J. Iron Steel Res. Int.*, 2011, vol. 18, pp. 52–58.
35. C. Garcia, L.F. Alvarez, and M. Carsi: *Weld. Int.*, 1992, vol. 6, pp. 612–21.
36. R.E. Dunin-Borkowski, J. Sloan, R.R. Meyer, A.I. Kirkland, and J.L. Hutchison, European JEOL Users Meeting, Jena, Germany 25-26 September 2000 (<http://www.rafaledb.com/papers/A-2000-09-Jena-JEOL-users-meeting-JEM-3000F-results.pdf>).
37. E.E. Underwood: *Quantitative Stereology*, Addison-Wesley Pub. Co., Atlanta, 1970, pp. 73–75.
38. G.F. Vander Voort and A. Roósz: *Metallography*, 1984, vol. 17, pp. 1–17.
39. H. Petitgand, D. Benoit, M. Moukassi, and B. Debyser: *SIJ Int.*, 1990, vol. 30, pp. 546–51.
40. F.G. Caballero, C. Garcia de Andres, and C. Capdevila: *Mater. Charact.*, 2000, vol. 45, pp. 111–16.
41. C. Yang, W. Zhang, H. Li, X. Chen, and Q. Zhai: *Characterization of Minerals, Metals, and Materials 2015*, Springer, Cham, 2016, pp. 601–06.
42. D. San Martin, Y. Palizdar, R.C. Cochrane, R. Brydson, and A.J. Scott: *Mater. Charact.*, 2010, vol. 61, pp. 584–88.
43. H. Torkamani, Sh. Raygan, C. Garcia Mateo, J. Rassizadehghani, Y. Palizdar, and D. San-Martin: *Met. Mater. Int.*, 2018.
44. D. San Martin, T. de Cock, A. Garcia-Junceda, F.G. Caballero, C. Capdevila, and C. García de Andrés: *Mater. Sci. Technol.*, 2008, vol. 24, pp. 266–72.
45. E. Kalinushkin, I. Mamuzic, Yu. Taran, and L. Tykhonuk: *METALURGIJA*, 2002, vol. 41 (3), pp. 131–38.
46. M. Wintz, M. Bobadilla, J. Lehmann, and H. Gaye: *SIJ Int.*, 1995, vol. 35, pp. 715–22.
47. Sh. Morioka and H. Suito: *SIJ Int.*, 2008, vol. 48, pp. 286–93.
48. H. Suito, H. Ohta, and S. Morioka: *SIJ Int.*, 2006, vol. 46, pp. 840–46.
49. G. Muxing and S. Hideaki: *SIJ Int.*, 1999, vol. 39, pp. 1289–96.
50. R. Tuttle: *IJMC*, 2012, vol. 6, pp. 51–65.
51. J. Lan, J. He, W. Ding, Q. Wang, and Y. Zhu: *SIJ Int.*, 2000, vol. 40, pp. 1275–82.
52. J. Gao, P. Fu, H. Liu, and D. Li: *Metals*, 2015, vol. 5, pp. 383–94.
53. H. Torkamani, Sh. Raygan, C. Garcia Mateo, J. Rassizadehghani, J. Vivas, Y. Palizdar, and D. San-Martin: *Metals*, 2017, vol. 7, pp. 377–95.
54. N. Fujiyama, T. Nishibata, A. Seki, H. Hirata, K. Kojima, and K. Ogawa: *Sci. Technol. Adv. Mater.*, 2017, vol. 18, pp. 88–95.
55. Z. Adabavazeh, W.S. Hwang, and A. Dezfoli: *Crystals*, 2017, vol. 7, pp. 308–17.
56. F. Pan, J. Zhang, H.L. Chen, Y.H. Su, C.L. Kou, Y.H. Su, S.H. Chen, K.J. Lin, P.H. Hsieh, and W.S. Hwang: *Materials*, 2016, vol. 9, pp. 417–36.

57. Zh.Q. Liu, G. Miyamoto, Zh.G. Yang, and T. Furuvara: *Metall. Mater. Trans. A*, 2013, vol. 44A, pp. 5456–67.
58. M. Umemoto and Z. Hai: Guo and I. Tamura *Mater. Sci. Technol.*, 1987, vol. 3, pp. 249–55.
59. M. Hillert: *Jernkontorets. Ann.*, 1957, vol. 141, pp. 757–46.
60. M. Hillert: *The Mechanism of Phase Transformation in Crystalline Solids*, Institute of Metals, London, 1969.
61. A.C. Reardon: *Metallurgy for the Non-Metallurgist*, 2nd ed., ASM International, Ohio, 2011.
62. T. Sakuma and R.W.K. Honeycombe: *Mater. Sci. Technol.*, 1985, vol. 1, pp. 351–56.
63. C. Capdevila, F.G. Caballero, and C. Garcia de Andres: *SIJ Int.*, 2005, vol. 45, pp. 229–37.
64. M. Atkins: *Atlas of Continuous Cooling Transformation Diagrams for Engineering Steels*, American Society for Metals, Ohio, 1980.
65. S.-J. Lee, D.K. Matlock, and C.J. Van Tyne: *Scripta Mater.*, 2011, vol. 64, pp. 805–08.
66. M. Martin-Aranda, R. Rementeria, R. Hackenberg, E. Urones-Garrote, S.P. Tsai, J.R. Yang, and C. Capdevila: *Materials*, 2016, vol. 9, pp. 998–1008.
67. M. Honjo, T. Kimura, and K. Hase: *SIJ Int.*, 2016, vol. 56, pp. 161–67.
68. Y. Wu, L. Wang, and T. Du: *JLCM*, 1985, vol. 110, pp. 187–93.
69. S.A. Al-Salman, G.W. Lorimer, and N. Ridley: *Metall. Trans. A*, 1979, vol. 10A, pp. 1703–09.
70. D.E. Coates: *Metall. Trans.*, 1972, vol. 3, pp. 1203–12.
71. D.E. Coates: *Metall. Trans.*, 1973, vol. 4, pp. 1077–86.
72. S.J. Lee, D.K. Matlock, and Ch.J. Van Tyne: *SIJ Int.*, 2011, vol. 51, pp. 1903–11.
73. X. Gao, H. Ren, C. Li, H. Wang, Y. Ji, and H. Tan: *J. Alloys Compd.*, 2016, vol. 663, pp. 316–20.
74. D.E. Laughlin and K. Hono: *Physical Metallurgy*, 5th ed., Elsevier, Amsterdam, 2014.
75. J.W. Cahn: *Acta Metall.*, 1959, vol. 7, pp. 18–28.
76. G.R. Speich and A. Szirmai: *Trans. TMS-AIME*, 1969, vol. 245, pp. 1063–74.
77. A. Jacot, M. Rappaz, and R.C. Reed: *Acta Mater.*, 1998, vol. 46, pp. 3949–62.
78. B.E. Sundquist: *Acta Metall.*, 1968, vol. 16, pp. 1413–27.
79. B.E. Sundquist: *Acta Metall.*, 1969, vol. 17, pp. 967–78.